Electronic Supplementary Information （*ESI*）

Anionic lanthanide metal-organic frameworks with magnetic, fluorescence, and proton conductivity properties and selective adsorption of a cationic dye

Xiao-Nuan Zhang, Bo-Chen Chen, Jia-Li Zhang, Jia-Lin Zhang, Sui-Jun Liu* and He-Rui Wen*

School of Chemistry and Chemical Engineering, Jiangxi Provincial Key Laboratory of Functional Molecular Materials Chemistry, Jiangxi University of Science and Technology, Ganzhou 341000, Jiangxi Province, P.R. China.

E-mail: wenherui63@163.com (He-Rui Wen); sjliu@jxust.edu.cn (Sui-Jun Liu)

Table S1. Selected bond lengths (Å) and angles (deg) for **1**[a].

Gd1—O1	2.301(4)	Gd1—O5^{iii}	2.456(5)
Gd1—O2^{i}	2.434(5)	Gd1—O6^{i}	2.524(5)
Gd1—O3^{ii}	2.311(4)	Gd1—O7^{iv}	2.371(5)
Gd1—O4^{iii}	2.452(4)	Gd1—O11^{v}	2.374(5)
O1—Gd1—O2^{i}	76.9(2)	O2^{i}—Gd1—O4^{iii}	98.6(2)
O1—Gd1—O3^{ii}	78.6(2)	O2^{i}—Gd1—O5^{iii}	71.1(2)
O1—Gd1—O4^{iii}	132.43(19)	O2^{i}—Gd1—O6^{i}	52.2(2)
O1—Gd1—O5^{iii}	82.15(18)	O3^{ii}—Gd1—O2^{i}	84.8(2)
O1—Gd1—O6^{i}	126.10(18)	O3^{ii}—Gd1—O4^{iii}	148.9(2)
O1—Gd1—O7^{iv}	79.78(18)	O3^{ii}—Gd1—O5^{iii}	152.0(2)
O1—Gd1—O11^{v}	135.34(15)	O3^{ii}—Gd1—O6^{i}	80.21(17)
O4^{iii}—Gd1—O5^{iii}	52.7(2)	O3^{ii}—Gd1—O7^{iv}	117.21(16)
O4^{iii}—Gd1—O6^{i}	77.81(17)	O5^{iii}—Gd1—O6^{i}	95.3(2)
O7^{iv}—Gd1—O2^{i}	143.7(2)	O11^{v}—Gd1—O2^{i}	137.64(19)
O7^{iv}—Gd1—O4^{iii}	77.43(17)	O11^{v}—Gd1—O4^{iii}	78.52(17)
O7^{iv}—Gd1—O5^{iii}	78.6(2)	O11^{v}—Gd1—O5^{iii}	129.2(2)
O7^{iv}—Gd1—O6^{i}	152.73(19)	O11^{v}—Gd1—O6^{i}	86.46(17)

[a]Symmetry codes: (i) −*x*+*y*, −*x*+1, *z*−1/3; (ii) −*x*+1, −*x*+*y*, −*z*+4/3; (iii) *y*−1, *x*, −*z*+1; (iv) −*x*, −*x*+*y*, −*z*+4/3; (v) *x*−1, *y*−1, *z*.

Table S2. Selected bond lengths (Å) and angles (deg) for **2**[b].

Dy01—O1^{i}	2.275(4)	Dy01—O4^{iv}	2.286(4)
Dy01—O8^{ii}	2.510(5)	Dy01—O5^{v}	2.443(5)
Dy01—O2^{iii}	2.350(5)	Dy01—O6^{v}	2.427(4)
Dy01—O3	2.349(4)	Dy01—O7^{ii}	2.400(5)
O1^{i}—Dy01—O2^{iii}	80.11(18)	O3—Dy01—O2^{iii}	77.14(19)
O1^{i}—Dy01—O3	135.12(15)	O3—Dy01—O5^{v}	128.93(19)
O1^{i}—Dy01—O4^{iv}	79.07(19)	O3—Dy01—O6^{v}	78.44(17)
O1^{i}—Dy01—O5^{v}	81.85(18)	O3—Dy01—O7^{ii}	138.05(18)
O1^{i}—Dy01—O6^{v}	132.92(19)	O3—Dy01—O8^{ii}	86.65(17)
O1^{i}—Dy01—O7^{ii}	76.88(18)	O4^{iv}—Dy01—O2^{iii}	118.29(16)
O1^{i}—Dy01—O8^{ii}	126.28(17)	O4^{iv}—Dy01—O3	78.5(2)
O2^{iii}—Dy01—O5^{v}	77.6(2)	O4^{iv}—Dy01—O5^{v}	152.2(2)
O2^{iii}—Dy01—O6^{v}	77.68(17)	O4^{iv}—Dy01—O6^{v}	147.8(2)
O2^{iii}—Dy01—O7^{ii}	143.7(2)	O4^{iv}—Dy01—O7^{ii}	84.4(2)
O2^{iii}—Dy01—O8^{ii}	152.17(18)	O4^{iv}—Dy01—O8^{ii}	79.48(18)
O5^{v}—Dy01—O8^{ii}	96.0(2)	O7^{ii}—Dy01—O5^{v}	71.6(2)
O7^{ii}—Dy01—O8^{ii}	52.44(19)	O7^{ii}—Dy01—O6^{v}	98.1(2)

[b]Symmetry codes: (i) *x*, *y*+1, z; (ii) −*x*+*y*+1, −*x*+2, *z*−1/3; (iii) *x*−*y*, −*y*+1, −*z*+2/3; (iv) *x*−*y*+1, −*y*+2, −*z*+2/3; (v) −*x*+1, -*x*+*y*+1, −*z*+1/3.

Table S3. RhB adsorption capacity and adsorption time of MOFs.

Dye	MOFs	Removalrate (mg/g)	Time (min)	Ref.
RhB	Ln-MOF **2**	79.42	40	this work
	MIL-125(Ti)	59.92	180	S1
	Zn-MOF	3.75	60	S2
	POM@UiO-66	222.6	120	S3
	USTC-1	13.4	240	S4
	MIL-68(Al)	1111.11	10	S5
	$MgFe_2O_4$@MOF	219.78	5	S6
	Fe_3O_4/MIL-100(Fe)	28.36	90	S7

Table S4. Maximum σ values of Ln-MOF **1** and RhB@Ln-MOF **1** compared with the selected Ln-MOFs.

MOFs	σ [$S\cdot cm^{-1}$]	conditions	E_a (eV)	Ref.
$H[(N(Me)_4)_2][Gd_3(NIPA)_6]\}\cdot 3H_2O$	7.17×10^{-2}	75 °C-98% RH	0.13	S8
$\{[Er_4(OH)_4(L)_2(H_2O)_8]\cdot 4.6H_2O\cdot 1.4CH_3CN\}_n$	6.59×10^{-3}	80 °C-95% RH	0.32	S9
$\{[Ho_4(OH)_4(L)_2(H_2O)_8]\cdot 4.6H_2O\cdot 1.4CH_3CN\}_n$	4.56×10^{-3}	80 °C-95% RH	0.38	S9
$\{[Dy(DMTP\text{-}DC)_{1.5}(H_2O)_3]\cdot H_2O\}_n$	2.67×10^{-4}	55 °C-100% RH	0.20	S10
$\{[Nd_2(HMIDC)_2(\mu_4\text{-}C_2O_4)(H_2O)_3]\cdot 4H_2O\}_n$	2.25×10^{-4}	100°C-98% RH	0.71	S11
$\{[Gd(DMTP\text{-}DC)_{1.5}(H_2O)_3]\cdot H_2O\}_n$	1.62×10^{-4}	55°C-100% RH	0.27	S10
Ln-MOF **1**	1.02×10^{-4}	50 °C -90% RH	0.34	this work
JXNU-8(Eu)	2.28×10^{-5}	80 °C-98% RH	0.18	S12
$\{[Gd_4(OH)_4(L)_2(H_2O)_8]\cdot 4.6H_2O\cdot 1.4CH_3CN\}_n$	2.02×10^{-6}	80 °C-95% RH	0.27	S9
RhB@Ln-MOF **1**	7.40×10^{-8}	50 °C -90% RH	0.45	this work

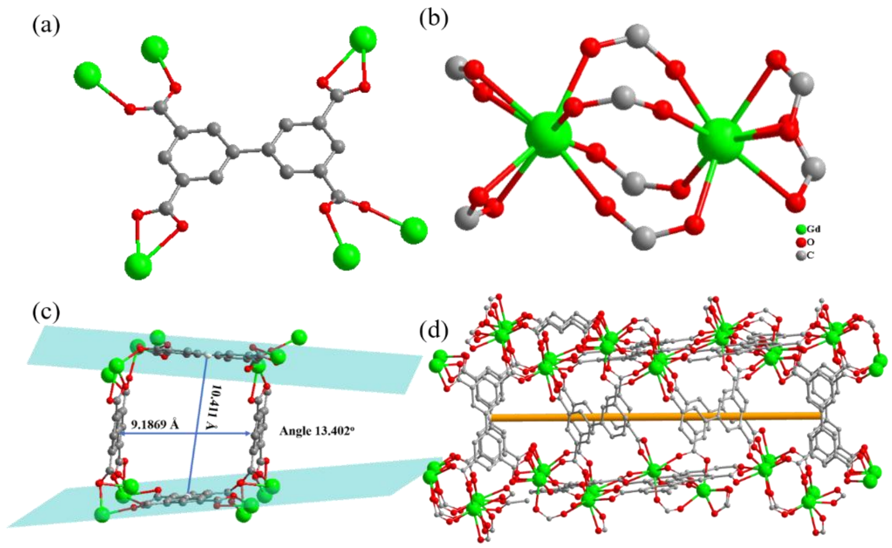

Fig. S1 (a) the way a metal is connected to a ligand; (b) Secondary building unit; (c) the dihedral angles and distances between ligands; (d) the 1D channel in Ln-MOF **1**.

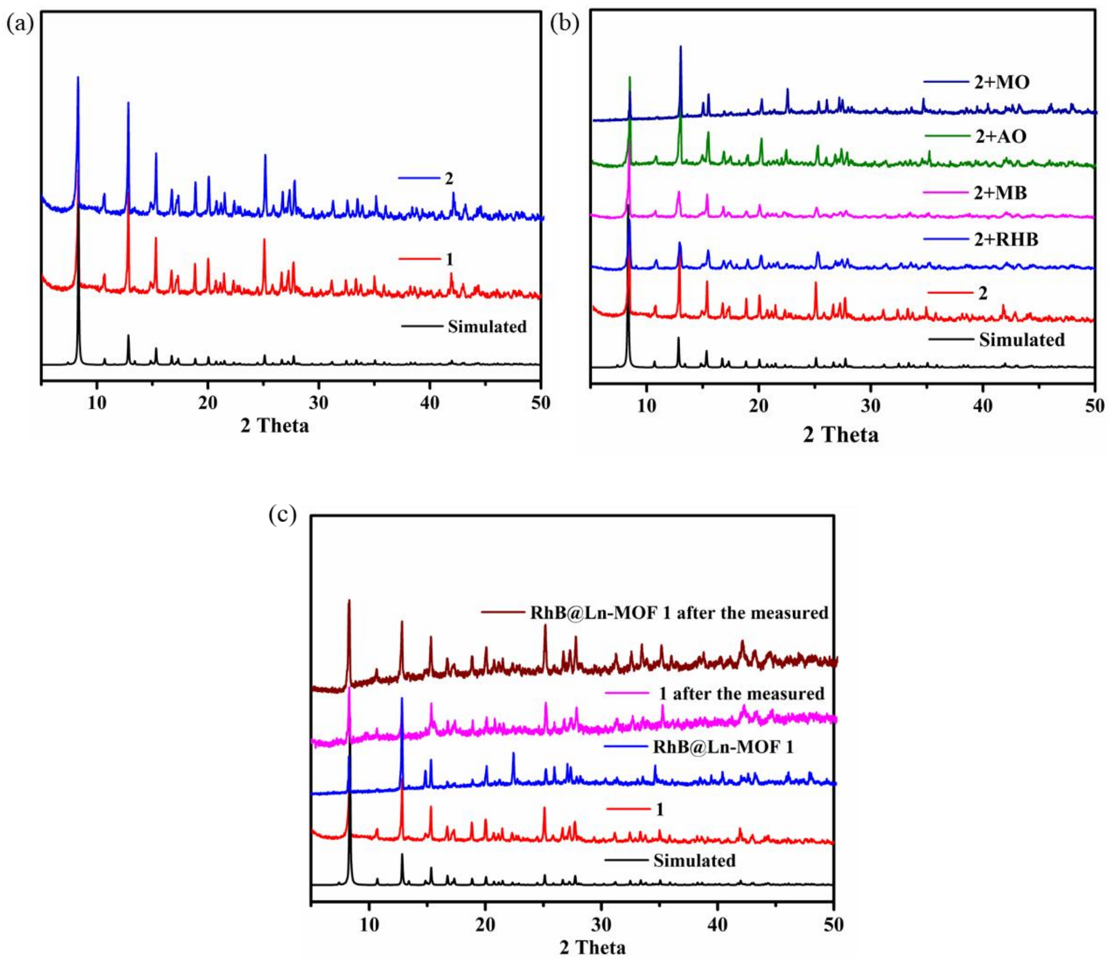

Fig. S2 The PXRD patterns of **1** and **2** (a), **2** after the adsorption of dyes (b), and RhB@Ln-MOF **1** and the sample after the proton conduction (c).

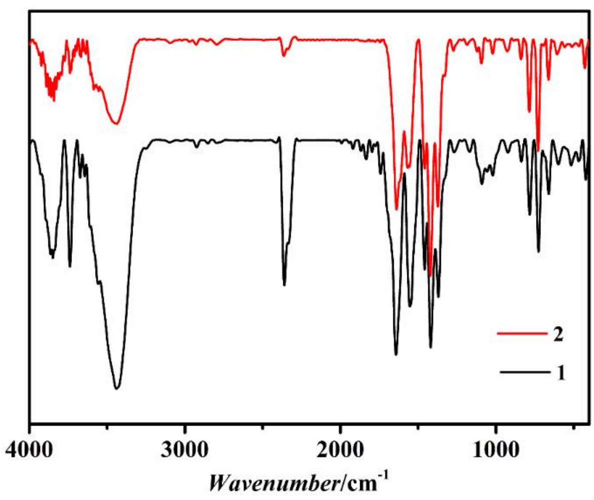

Fig. S3 The IR spectra of Ln-MOFs **1** and **2**.

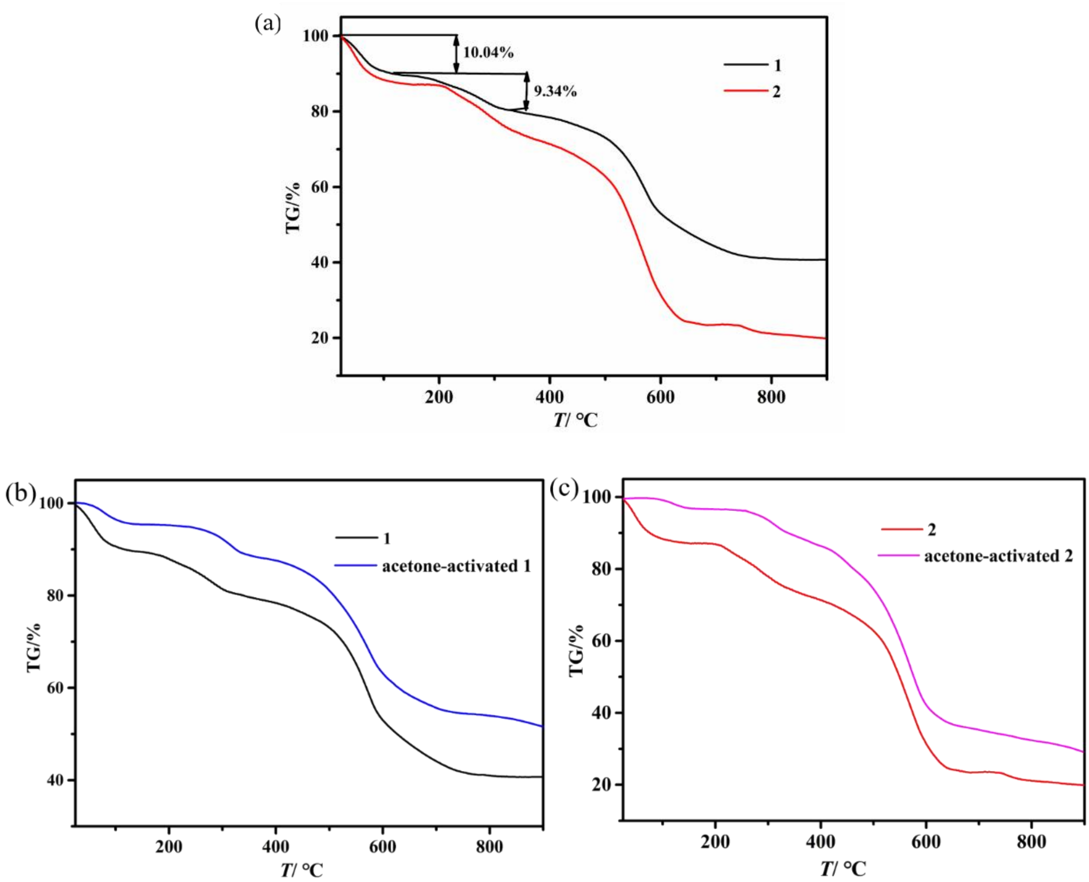

Fig. S4 The TG curves of Ln-MOFs **1** and **2** (a), and acetone-activated **1** (b) and **2** (c).

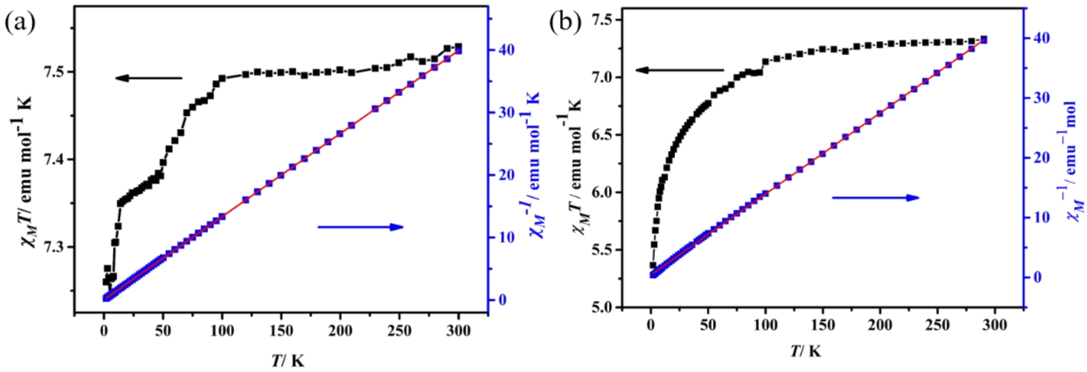

Fig. S5 Plots of $\chi_M T$ vs T and χ_M^{-1} vs T of Ln-MOFs **1** (a) and **2** (b). Red lines for the Curie-Weiss fitting.

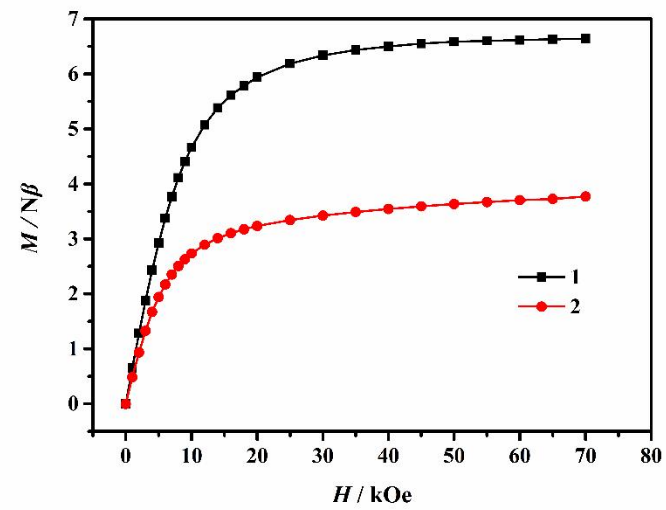

Fig. S6 Field dependence of the magnetizations of **1** and **2** at 2 K.

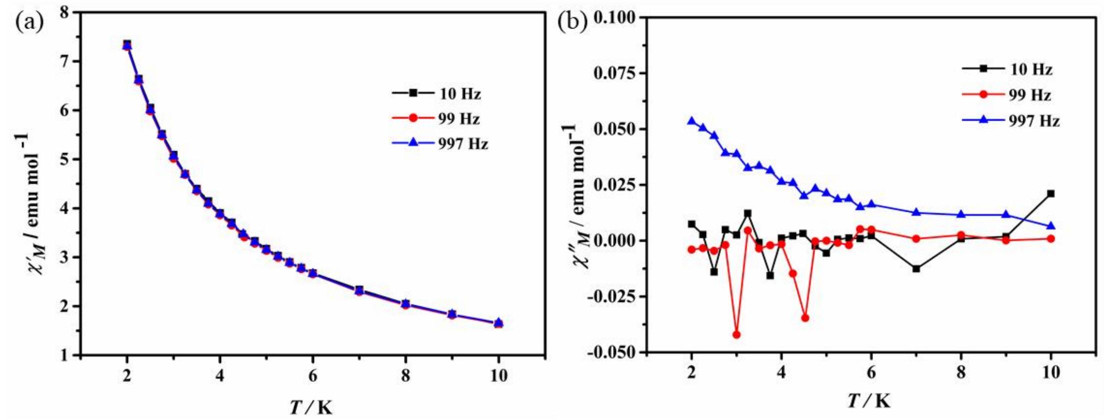

Fig. S7 Frequency dependence of the in-phase (χ') and out-of-phase (χ'') ac susceptibility signals for **2** under zero-dc field.

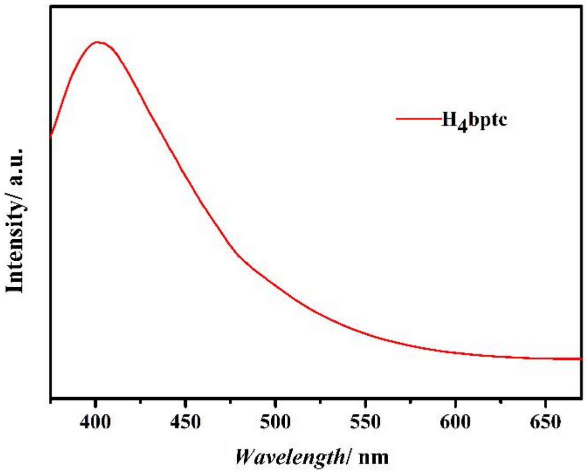

Fig. S8 The emission spectrum of H_4bptc (λ_{ex} = 354 nm).

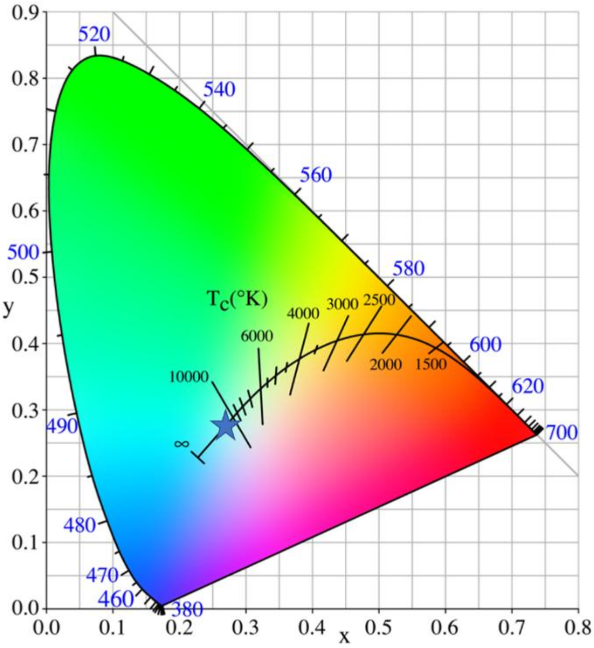

Fig. S9 CIE chromaticity diagram showing the color coordinates of Ln-MOF **2** under the excitation of 328 nm.

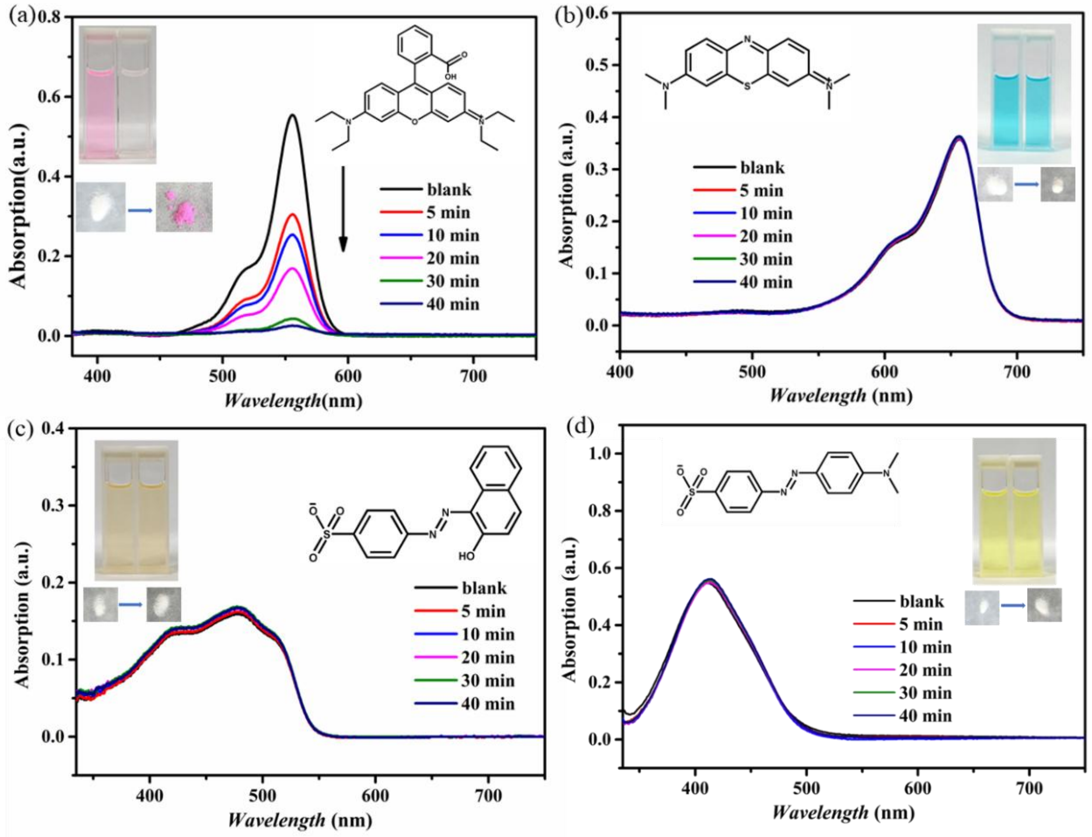

Fig. S10 UV−vis absorption spectra of **1** adsorbed RhB (a), MB (b), AO (c) and MO (d) in acetone solutions during the adsorption process.

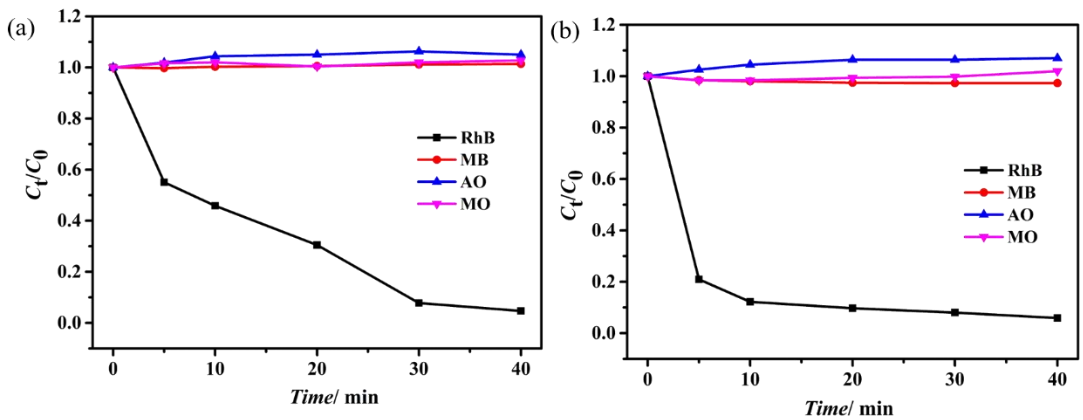

Fig. S11 Corresponding plots of C_t/C_0 of dyes versus time during the adsorption of **1** (a) and **2** (b).

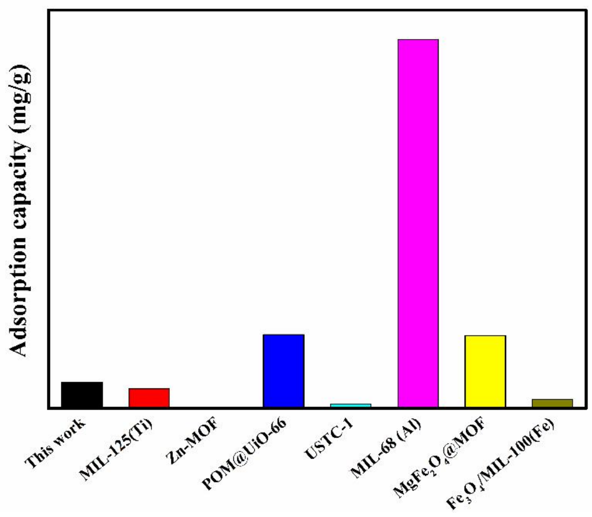

Fig. S12 The RhB adsorption capacity of different MOFs.

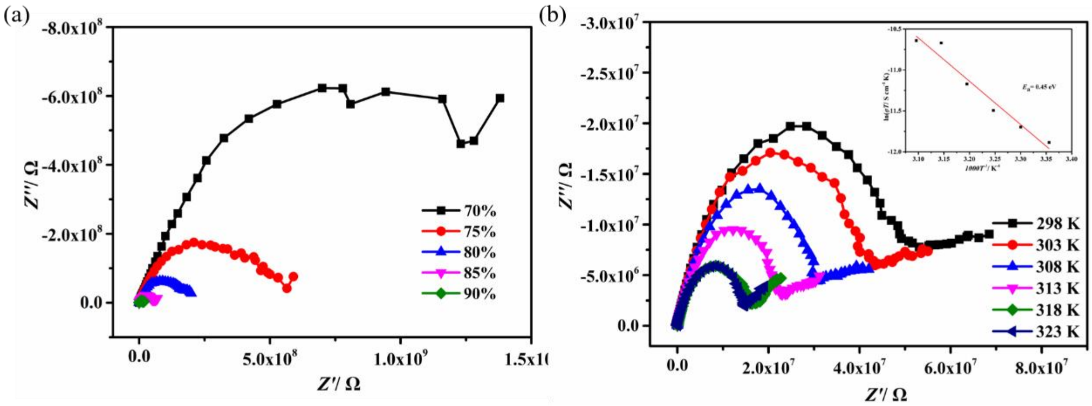

Fig. S13 (a) Nyquist plots for RhB@Ln-MOF **1** at different RHs and T = 323 K. (b) Nyquist plots for RhB@Ln-MOF **1** at different temperatures and 90% RH; Arrhenius plots of the conductivity of RhB@Ln-MOF **1** (inset).

References

S1 H. Guo, F. Lin, J. Chen, F. Li and W. Weng, *Appl. Organomet. Chem*., 2015, **29**, 12–19.

S2 J. Zhang, F. Li and Q. Sun, *Appl. Surf. Sci. J.*, 2018, **440**, 1219–1226.

S3 L. Zeng, L. Xiao, Y. Long and X. J. Shi, *Colloid Interface Sci*., 2018, **516**, 274–283.

S4 B. Li, W. Jiang, Y. Xu, Z. Xu, Q. Yan and G. Yong, *Dyes Pigments*, 2020, **174**, 108017.

S5 M. S. Tehrani and R. Zare-dorabei, *RSC Adv*., 2016, **6**, 27416–27425.

S6 H. Tian, J. Peng, T. Lv, C. Sun and H. J. He, *Solid State Chem*., 2018, **257**, 40–48.

S7 H. Liu, X. Ren and L. Chen, *J. Ind. Eng. Chem*., 2016, **34**, 278–285.

S8 X. S. Xing, Z. H. Fu, N. N. Zhang, X. Q. Yu, M. S. Wang and G. C. Guo, *Chem. Commun*., 2019, **55**, 1241−1244.

S9 S. P. Bera, A. Mondal, S. Roy, B. Dey, A. Santra and S. Konar, *Dalton Trans*., 2018, **47**, 15405−15415.

S10 J. J. Hu, Y. G. Li, H. R. Wen, S. J. Liu, Y. Peng and C. M. Liu, *Inorg. Chem*., 2022, **61**, 6819-6828.

S11 R. L. Liu, Y. H. Yu, H. W. Wang, Y. Y. Liu and G. Li, *Inorg. Chem*., 2021, **60**, 10808−10818.

S12 M. Y. Xu, Y. L. Wang, Q. Y. Liu, Z. T. Lin and Q. Y. Liu, *Inorg. Chem*., 2020, **59**, 7265−7273.